Optimal shape and stress control of geometrically nonlinear structures with exact gradient with respect to the actuation inputs

Ahmed Manguri [a,b], Domenico Magisano [c,*], Robert Jankowski [a]

[a] *Faculty of Civil and Environmental Engineering, Gdansk University of Technology, Gdansk, Poland*
[b] *Civil Engineering Department, University of Raparin, Rania, Iraq*
[c] *Department of Computer Science, Modeling, Electronics and Systems Engineering, University of Calabria, Rende (Cosenza), Italy*

ABSTRACT

This paper presents an efficient and robust optimization methodology for stress and shape control of actuated geometrically nonlinear elastic structures, applied to 3D trusses. The actuation inputs, modeled as prescribed strains, serve as the optimization variables. The objective is to minimize total actuation while satisfying several constraints: (i) actuation bounds in each actuated element and (ii) target ranges for nodal displacements and element stresses. Optimizing large nonlinear structures is computationally intensive. While gradient-based methods typically converge faster than gradient-free ones, their main bottleneck lies in numerical gradient evaluation, requiring multiple time-consuming nonlinear structural analyses (finite differences) with inaccuracies that may slow down convergence. The novelty of the proposal is an implicit differentiation approach to quickly compute the exact gradient of the nonlinear finite element solution with respect to the actuation inputs. This is implemented within the structural solver and leverages the already factorized tangent stiffness matrix to make the gradient cost negligible. As a result, the number of structural analyses and overall optimization time are significantly reduced.

1. Introduction

Geometrically nonlinear structures are characterized by significant deformations, and the deformed geometry considerably influences their stiffness and strength. They are becoming increasingly common in various engineering applications, including aerospace, civil, naval, and mechanical engineering.

Structures, particularly those supporting sensitive equipment for communication and scientific purposes, often undergo large deformations when subjected to unexpected loading or harsh environments. In these cases, shape control becomes paramount [1,2]. Active shape control is essential for flexible space structures, such as antenna reflectors and solar sails, to meet specific mission objectives, including shape accuracy and adaptability to different operational conditions [3]. On the other hand, structures like cable bridges and tensegrities require heightened emphasis on regulating internal forces within their components, rather than focusing solely on deformations. This is particularly evident in configurations featuring cable elements, which may experience slackness under specific loads, necessitating adjustments to maintain their structural integrity [4]. In real-world applications, manipulating a single variable without concomitant effects on other variables poses a considerable challenge. For instance, when restoring

an antenna to a predetermined shape by adjusting the lengths of specific members, caution must be exercised to prevent the generation of hazardous levels of strut forces or the slackening of cables due to diminished internal force. Achieving this delicate balance requires controlling nodal displacements and bar forces, a task that is often inherently intricate [5]. Shape and stress control are achieved by changing the length of some active bars using a device called an actuator [6]. Various types of actuators, such as mechanical [7], shape memory alloy [8], and piezoelectric actuators [9–11], are employed.

The idea of structural control was presented on a flexible beam [12] and a large space antenna [13], which then further developed analytically [14]. In a comprehensive review [15], the control of structural shape and stress and the optimization of various actuators were extensively discussed, covering key advancements and applications in the field. The shape and stress control of geometrically nonlinear structures pose a challenging problem due to the complex nonlinear relationships between geometry, loading, and deformation. Traditional design and analysis methods based on linear elasticity are often inadequate. In recent years, there has been a growing interest in developing new methods for the shape and stress control of flexible structures. Some of these methods are based on linear methods but are not valid for

* Corresponding author.
E-mail addresses: ahmed.manguri@pg.edu.pl (A. Manguri), domenico.magisano@unical.it (D. Magisano), jankowr@pg.edu.pl (R. Jankowski).

large displacements. In an experimental study, the displacement of a specific nod was controlled [16]. Then the study was extended to simultaneously control nodal displacement and internal bar forces of linear truss structures [17,18]. A study compared two equivalent methods, the integrated force method (IFM) and the singular value decomposition approach (SVD-FM) [19]. On the other hand, techniques based on nonlinear methods [20,21] may require significant computational time and may be affected by a lack of robustness. Another limitation of previous studies on shape and stress control is the requirement for a significant amount of actuation which this study also aims to address.

Optimization is defined as the process of finding the best possible solution for a given problem [22], opening a new chapter in structural engineering [23]. In structural engineering, optimization is implemented for one or more purposes, such as minimizing material usage and overall cost [24], or improving structural resistance [25]. Additionally, structural optimization has been implemented for topology optimization, considering thermal effects and initial imperfections [26] and maintaining the structural integrity and performance [27]. A constructability-based optimization method for steel trusses is proposed. Using a penalty approach, complexity is minimized, and the Howe truss is identified as the optimal solution for a real 3D roof structure [28]. Optimization algorithms can minimize the number of actuators and actuation in adaptive structures [29,30]. Adaptive structures can achieve significant whole-life energy savings by using controlled shape changes to redistribute stress, optimize material usage, and reduce embodied energy, as demonstrated through experimental testing of a small-scale planar truss prototype by actuating active actuators [31].

Structural geometry and properties can be changed in real-time as an actuation system to maintain the desired shape and stress distribution. For geometrically linear and nonlinear trusses, a weight optimization method based on the gradient and two sub-problems is proposed in [32] by reformulating the optimization problem in displacement variables. Gradient-based optimizations of shells prone to buckling are also developed in [33,34], exploiting a reduced order model of the structure to reduce the computational time. The computation of the gradients, generally possible only by numerical differentiation, is the bottleneck in nonlinear design optimization, as addressed in [35] exploiting parallel computing. Alternative metaheuristic approaches based, for example, on the genetic algorithm and the mine blast algorithm are also available [36,37]. The algorithm was used to optimize the number, spatial arrangement, and sizing of steel exoskeletons for seismic retrofitting by minimizing weight and ensuring structural elasticity. Performance was evaluated through finite-element analysis and case studies, demonstrating significant reductions in weight and cost [38]. A novel inverse method utilizes metaheuristic algorithms to optimize strain data from distributed fiber optic sensors [39]. This method helps in determining real strain distributions and solving interfacial mechanics, which in turn improves the understanding of strain transfer, debonding behavior, and structural health monitoring [40]. The greater flexibility of gradient-free methods in global optimization compared to gradient-based ones is, however, usually counterbalanced by the greater number of function evaluations in the former, especially when a closed-form gradient is available. Moreover, gradient-free methods scale very poorly with the dimensionality of the design space.

This work considers prescribed strains as actuation systems [41]. These are often achieved mechanically. However, it is worth noting that more complex actuation systems, such as temperature change [42,43], and illumination [44], can be also modeled as assigned strains. Similar considerations apply to biological and bio-hybrid structures, where electrophysiological stimuli are converted into mechanical actions based on the active strain approach [45]. Recent works also demonstrate that small beneficial geometric deviations can nudge structures onto favorable equilibrium paths [46], and they can be modeled as equivalent prescribed strains, as shown in [47,48].

This research presents a gradient-based optimization technique integrated with the nonlinear finite element method to minimize actuation for controlling both the deformed shape and stress in geometrically nonlinear structures. The study specifically addresses the quasi-static case. The objective function, representing the total actuation, is minimized using a gradient-based Sequential Quadratic Programming algorithm [49]. The constraints include target nodal positions and/or stress in structural elements, as well as actuation bounds in each actuated element. The weak point of standard optimization tools is that the gradient of nonlinear constraints, i.e., deformed shape and stress, is usually computed approximately through numerical differentiation. The aim of this article is to overcome this weak point, demonstrating how the exact gradient of the nonlinear finite element solution can be evaluated within the structural solver robustly and at a negligible computational cost. The theory behind the developments relies on the chain implicit differentiation and the exploitation of the tangent stiffness matrix already factorized in the structural Newton iterations. As a result, the optimal design of the actuation system is made robust and efficient, especially for structures with many degrees of freedom. The procedure is illustrated for 3D trusses, from small to large structures, due to the simplicity of the models and implementation which are easy to reproduce by interested readers. However, the approach is formulated to apply to any geometrically nonlinear finite element model, using a general formal of discrete equations to facilitate the integration within commercial codes.

The paper is organized as follows: Section 2 describes the geometrically nonlinear problem with reference to a finite element model for 3D trusses with actuation modeled as prescribed strains in some actuated elements, introducing the necessary notation. Section 3 is the core of this work, formulating and addressing the nonlinear optimization problem for displacement and stress control using a gradient-based method. Special attention is given to differentiating displacement and stress coming from the nonlinear finite element solution with respect to the actuation parameters. Section 4 demonstrates the gain in robustness and efficiency achieved in the optimization algorithm using the exact closed-from differentiation strategy compared to the standard numerical differentiation. The reduction of computational time is also discussed for large structures. Conclusions are reported in the last section.

2. The 3D truss model with actuators and initial stresses

The optimization process developed in this work can be applied to generic large deformation structural models with elastic materials discretized by the finite element method. The hypotheses of the work are:

- quasi-static problem;
- finite kinematics with nonlinear strain–displacement relationship;

- equilibrium in the deformed configuration;
- hyperelastic materials.

To simplify the exposition as much as possible and make the procedure easy for the reader to understand, 3D truss structures are considered simple examples of applications where each finite element coincides with the physical bar. This also makes the numerical results very easy to reproduce.

This section recalls the nonlinear discrete equations of a large deformation truss model based on the quadratic Green–Lagrange strain measure. The model is introduced, as usual, starting from the variational problem formulated in a displacement-based approach. Thus, the nonlinear equilibrium equations are derived and the incremental-iterative solution scheme is quickly discussed. This information will be of help for the subsequent developments.

It is worth noting that introducing a general finite element context aims to show that the developments are not influenced by the structural
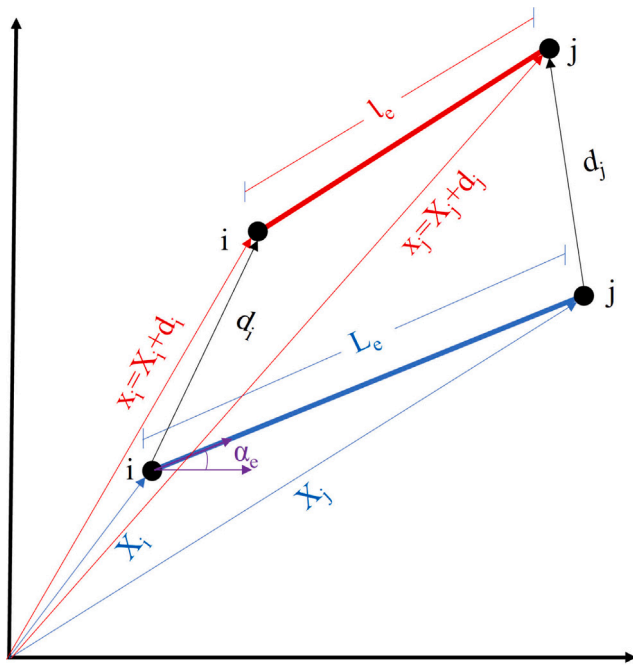
Fig. 1. Kinematics of the bar element.

topology, e.g., geometry, number of nodes, and elements. Conversely, the exact gradient evaluation method developed in the subsequent section can be easily and efficiently integrated within any commercial structural software under the hypotheses listed above. Also, the discrete equations of the finite element model have an identical format as those coming from other structural models (beams/frames, plates/shells, 3D continuum), making the methodology extensible to different structural types.

2.1. The truss element: kinematics and strain measure

The position of the two end-nodes (i and j) of the generic bar (see Fig. 1) in the reference (initial) and current configuration is denoted as $\mathbf{X}_k$ and $\mathbf{x}_k$ respectively, with $k = i, j$. The kinematics of each node can be then expressed as

$$\mathbf{x}_k = \mathbf{X}_k + \mathbf{d}_k$$

where $\mathbf{d}_k$ denotes the displacement of the kth node. For each truss element (bar), it is useful to introduce the following vectors

$$\Delta\mathbf{X}_e \equiv \mathbf{X}_j - \mathbf{X}_i \quad \text{and} \quad \Delta\mathbf{x}_e \equiv \mathbf{x}_j - \mathbf{x}_i = \Delta\mathbf{X}_e + \mathbf{d}_j - \mathbf{d}_i$$

The initial L_e and final ℓ_e lengths of the bar are obtained as

$$L_e^2 = \Delta\mathbf{X}_e^T \Delta\mathbf{X}_e$$
$$\ell_e^2 = \Delta\mathbf{x}_e^T \Delta\mathbf{x}_e = L_e^2 + 2\Delta\mathbf{X}_e^T(\mathbf{d}_j - \mathbf{d}_i) + (\mathbf{d}_j - \mathbf{d}_i)^T(\mathbf{d}_j - \mathbf{d}_i)$$

The Green–Lagrange strain measure expressing the strain–displacement compatibility is

$$\varepsilon_d(\mathbf{d}_e) = \frac{1}{2}\left(\frac{\ell_e^2}{L_e^2} - 1\right) = \frac{1}{L_e}\boldsymbol{\alpha}_e^T(\mathbf{d}_j - \mathbf{d}_i) + \frac{1}{2L_e^2}(\mathbf{d}_j - \mathbf{d}_i)^T(\mathbf{d}_j - \mathbf{d}_i) \quad (1)$$

where $\boldsymbol{\alpha}_e = \dfrac{\Delta\mathbf{X}_e}{L_e}$ is the vector containing the cosines directors of the bar generically oriented in a 3D space. Using a standard FE notation, we introduce the element vector $\mathbf{d}_e$

$$\mathbf{d}_e = \begin{bmatrix} \mathbf{d}_i \\ \mathbf{d}_j \end{bmatrix}$$

collecting the 6 discrete displacement DOFs of the bar corresponding to the nodal displacements. The Green–Lagrange strain in Eq. (1) rewrites as

$$\varepsilon_d = \frac{1}{L_e}\left(\mathbf{b}_e^T\mathbf{d}_e + \frac{1}{2}\mathbf{d}_e^T\mathbf{G}_e\mathbf{d}_e\right) \quad (2)$$

where

$$\mathbf{b}_e = \begin{bmatrix} -\boldsymbol{\alpha}_e \\ \boldsymbol{\alpha}_e \end{bmatrix} \quad \text{and} \quad \mathbf{G}_e = \frac{1}{L_e}\begin{bmatrix} \mathbf{I} & -\mathbf{I} \\ -\mathbf{I} & \mathbf{I} \end{bmatrix}$$

and $\mathbf{I}$ is the 3×3 identity matrix. The total strain ε_d coming from the displacement can be decomposed, assuming large deformations with small strains, as a sum of an elastic part ε and inelastic prescribed strains ε_0 and ε_a:

$$\varepsilon_d(\mathbf{d}_e) = \varepsilon + \varepsilon_0 + \varepsilon_a \quad (3)$$

where ε_0 is an initial pre-strain and ε_a is the strain induced by the actuators, which will the object of the design i.e. the variable of the optimization problem. Consequently, the axial force in the bar can be written as

$$N = EA\varepsilon = EA(\varepsilon_d(\mathbf{d}_e) - \varepsilon_0 - \varepsilon_a) \quad (4)$$

or, alternatively, as

$$N = EA\varepsilon = EA(\varepsilon_d(\mathbf{d}_e) - \varepsilon_a) + N_0 \quad \text{with} \quad N_0 = -EA\varepsilon_0 \quad (5)$$

where N_0 represents a possible axial force imposed as pre-stress before the actuation.

2.2. The equilibrium condition: internal force vector and stiffness matrix

The strain energy of the structures is obtained by summing the contribution, denoted as Φ_e, of each bar finite element:

$$\Phi = \sum_e \Phi_e \quad \text{where} \quad \Phi_e = \frac{1}{2}EAL_e(\varepsilon - \varepsilon_0 - \varepsilon_a)^2 \quad (6)$$

The internal force vector of the element is evaluated as the gradient of the element strain energy

$$\mathbf{s}_e = \frac{\partial\Phi_e}{\partial\mathbf{d}_e} = N\mathbf{q}_e \quad \text{with} \quad \mathbf{q}_e = \mathbf{b}_e + \mathbf{G}_e\mathbf{d}_e \quad (7)$$

with $N = EA(\varepsilon - \varepsilon_0 - \varepsilon_a)$. The Hessian of Φ_e furnishes the tangent stiffness matrix of the element

$$K_e = \frac{\partial^2\Phi_e}{\partial\mathbf{d}_e^2} = \frac{EA}{L_e}\mathbf{q}_e\mathbf{q}_e^T + N_e\mathbf{G}_e \quad (8)$$

Letting $\mathbf{p}_k$ represent the forces acting at the kth node of the entire structure, the external work is the sum of the nodal contributions:

$$\mathcal{L}_{ext} \equiv \sum_{k=1}^{N_n} \mathbf{p}_k^T\mathbf{d}_k = \mathbf{p}^T\mathbf{d}$$

where $\mathbf{d}$ is the global vector collecting all the nodal displacement DOFs of the structure. The total potential energy is the sum of the strain energy of all elements and the external work:

$$\Pi(\mathbf{d}) = \sum_e \Phi_e - \mathbf{p}^T\mathbf{d}. \quad (9)$$

The nonlinear equilibrium equations are obtained from the stationary condition of Π:

$$\frac{\partial\Pi}{\partial\mathbf{d}} = \mathbf{s}(\mathbf{d}) - \mathbf{p} = \mathbf{0} \quad \text{with} \quad \mathbf{s}(\mathbf{d}) = \sum_e \mathbf{T}_e^T\mathbf{s}_e(\mathbf{d}_e) \quad (10)$$

where $\mathbf{T}_e$ is the incidence matrix used for the global assembly of the element contributions, so that $\mathbf{d}_e = \mathbf{T}_e\mathbf{d}$. In a similar fashion, we obtain the global tangent matrix that will be used in the iterative solution method

$$K = \sum_e \mathbf{T}_e^T K_e \mathbf{T}_e.$$

2.3. Incremental-iterative solution

The equilibrium of slender elastic structures subject to conservative loads amplified by a proportionality factor λ is expressed by Eq. (10)

$$\mathbf{r}(\mathbf{d}, \lambda) \equiv \mathbf{s}(\mathbf{d}) - \lambda \mathbf{p} = \mathbf{0} \tag{11}$$

where $\mathbf{r} : \mathbb{R}^{n+1} \to \mathbb{R}^n$ is a nonlinear vectorial function of the vector $(\mathbf{d}, \lambda)$, collecting the configuration $\mathbf{d} \in \mathbb{R}^n$ and the load multiplier $\lambda \in \mathbb{R}$, $\mathbf{s}(\mathbf{d})$ is the global internal force vector and $\mathbf{p}$ the reference load vector. Eq. (11) represents a system of equations and unknowns and its solutions define the equilibrium path as a load factor-displacement curve in $\mathbb{R}^{n+1}$. An incremental-iterative solution scheme can be adopted to trace this curve in a step-by-step manner from a known initial configuration corresponding to $\lambda = 0$. The condition $\lambda = 1$ corresponds to the actual reference load of interest. There are two main reasons for introducing the load factor λ: (i) the equilibrium curve can exhibit a limit point in λ, meaning that there may be no close equilibrated solution above a certain load level; (ii) even if an equilibrium point exists for all λ in the range of interest, it is not assured that we are actually able to compute it directly for an assigned load. Regarding the first issue, the Riks arc-length method [50] can be used for dealing with limit points. Instead, for simplicity of exposition, we focus here on the second case.

An incremental solution scheme can be applied by defining a sequence of points (steps) $\mathbf{z}^{(k)} \equiv (\mathbf{d}^{(k)}, \lambda^{(k)})$ belonging to the equilibrium path. Starting from a known equilibrium point $\mathbf{z}_0 \equiv \mathbf{z}^{(k)}$, the new one $\mathbf{z}^{(k+1)}$ is evaluated correcting a first prediction of the displacement DOFs $\mathbf{d}_1$ corresponding to $\lambda^{(k+1)}$ by a sequence of estimates $\mathbf{d}^j$ by Newton iterations

$$\mathbf{d}_{j+1} = \mathbf{d}_j + \dot{\mathbf{d}} \quad \text{with} \quad \dot{\mathbf{d}} = -K(\mathbf{d}_j)^{-1} \mathbf{r}(\mathbf{d}_j, \lambda^{(k+1)}) \tag{12}$$

At each Newton iteration of each load step the global tangent stiffness matrix, obtained by assembling the element ones in Eq. (8), is computed and factorized for solving the linear systems. This operation is usually the costliest one in the analysis of large structures. The Newton iteration terminates when the norm of the residual vector $\mathbf{r}$ falls below a small predefined threshold.

The convergence of the Newton scheme is local, i.e. it converges when a good initial prediction of the unknowns (the displacement DOFs) is available. Clearly, this is not guaranteed for large load steps. Thus, the stepping procedure is useful for problems with a significant nonlinearity. Reaching the maximum load level in multiple steps allows one to take advantage of the previous equilibrium points in estimating the new one. A typical choice is to extrapolate linearly the two previous points for estimating the newly searched one. The number of load steps can be selected by the user, but can be adjusted automatically following, for example, the adaptive stepping reported in [51]. Clearly, in the present case of an elastic structure under a conservative load, the solution for the final load is unaffected by the stepping scheme (loading path). A mixed solution scheme involving also local stress variables to improve the robustness of the Newton scheme and to reduce the number of iterations [51,52].

3. Optimization: problem statement, solver and gradient evaluation

This section is dedicated to formulating the optimization problem for displacement and stress control in the context of geometrically nonlinear problems, along with its solution strategy. The emphasis is placed on differentiating the nonlinear finite element solution with respect to the actuation inputs to achieve an efficient and robust gradient-based optimization. Sequential Quadratic Programming is selected as the optimization algorithm.

3.1. Problem statement

To compare pure results with what is typically done in the literature, we consider as optimization variables the actuation in terms of prescribed elongation a instead of the axial strain ε_a:

$$a = \varepsilon_a L \tag{13}$$

where L is the length of the generic actuated element. The optimization problem for displacement and stress control of a geometrically nonlinear structure can be formulated as the minimization of the total actuation inputs (prescribed elongations) subject to the following constraints:

- upper and lower bound for the actuation a in each actuated bar;
- upper and lower bound for the stress in controlled elements coming from the nonlinear finite element model with the prescribed actuation;
- upper and lower bound for the displacement of controlled nodes coming from the nonlinear finite element model with the prescribed actuation.

This can be summarized as the following optimization problem:

$$
\begin{aligned}
&\text{minimize} && \sum_{i \in \mathcal{U}} |a_i| \\
&\text{subject to} && d_k^{(\min)} \leq d_k(\mathbf{a}) \leq d_k^{(\max)} && k \in \mathcal{K} \\
& && N_e^{(\min)} \leq N_e(\mathbf{a}) \leq N_e^{(\max)} && e \in \mathcal{E} \\
& && a_i^{(\min)} \leq a_i \leq a_i^{(\max)} && i \in \mathcal{U}
\end{aligned}
\tag{14}
$$

where $\mathbf{a}$ collects all the actuation inputs. $\mathbf{d}(\mathbf{a})$ and $N_e(\mathbf{a})$ are implicitly defined as those which verify the nonlinear structural equilibrium equations in Eq. (10) for given $\mathbf{a}$, this means that each evaluation of the constraints requires a nonlinear structural analysis according to Section 2.3 for the given load and actuation. Subsets $\mathcal{U}$, $\mathcal{E}$ and $\mathcal{K}$ denote, respectively, the actuated elements, the elements where we want to control the axial force N_e (stress resultant) and the controlled nodal displacement components d_k chosen among those the global vector $\mathbf{d}$ of displacement DOFs.

The number of optimization variables is the size of vector $\mathbf{a}$ corresponding to the cardinality of $\mathcal{U}$. The same value is also the number of linear constraints. Instead, the number of nonlinear constraints depends on the number of elements and nodal displacement components to control, i.e. the sum of the cardinality of $\mathcal{E}$ and $\mathcal{K}$.

It is worth remembering that, for generic statically indeterminate structures, even changing one of the actuation inputs in an element produces different displacements and axial forces in all the structural elements.

3.2. Optimization algorithm

The solution of the optimization problem (Eq. (14)) is tackled by using the Sequential Quadratic Programming method [49] implemented in *MATLAB* in the function named *fmincon* and activated by setting SQP as the solution algorithm. This is the state-of-art iterative method for constrained nonlinear optimization which may be seen as a quasi-Newton method. The main idea behind SQP is to approximate the problem (Eq. (14)) at each iterate with a local quadratic model of the objective function subject to a linearization of the constraints, i.e. a simpler Quadratic Programming. Importantly, the method requires an accurate gradient of the Lagrangian function, namely the gradient of objective function and constraints, while a positive definite quasi-Newton approximation of the Hessian of the Lagrangian function is typically employed.

In our optimization problem, the analytical gradient of the objective function is derived very easily. Instead, the gradient of the nonlinear constraints is more complicated since it involves the differentiation of the nonlinear structural response (finite element solution) in terms of stress and displacement with respect to the actuation inputs. The

standard approach uses a numerical differentiation to approximate these derivatives with either forward (default in *fmincon*) or central difference formulas. This means that the gradient evaluation requires a huge number of nonlinear structural analyses, at least one for each of the optimization variables. For structures with a large number of DOFs, this part is the bottleneck of the algorithm, mainly dominating the overall computational time with the repeated evaluation and factorization of the tangent stiffness matrix in the Newton iterations for imposing the structural equilibrium. In addition, it is necessary to consider the well-known trade-off of finite differences: the increment must be small enough for approximating the derivatives, but not too small to avoid round-off errors due to the limited machine precision. Since the nonlinear equilibrium equations are solved iteratively, the accuracy of the numerical differentiation can also be affected by the threshold of the structural iterative solver. As a consequence, the overall numerical approximation in the gradient evaluation can affect negatively the convergence of the optimization process, producing an increment of iterations of the optimization algorithm. Ultimately, both evaluation cost and accuracy of the gradient are relevant factors affecting the design procedure. The next subsection represents the main novelty point of this work, where an alternative closed-form differentiation of both displacement and stress of the nonlinear finite element model with respect to the actuation inputs is derived. The result provides a significant speed-up of the optimization process.

3.3. Gradient of the nonlinear finite element solution with respect to the actuation inputs

The goal is to calculate the gradient of the global vector $\mathbf{d}(\mathbf{a})$, which collects the displacement components of all nodes of the structures at their final equilibrium configuration for assigned final loads and actuation. This gradient is computed with respect to the optimization variables, namely the actuation inputs represented by the elongation values in the actuated elements collected in vector $\mathbf{a}$. Subsequently, these derivatives, denoted as $\nabla_{\mathbf{a}}\mathbf{d}$, can be utilized to derive $\nabla_{\mathbf{a}}N$, enabling the differentiation of the final axial force in each element e.

The difficulty of an analytical differentiation relies on the fact that no explicit expression for $\mathbf{d}(\mathbf{a})$ and $N(\mathbf{a})$ is available. All we know is that $\mathbf{d}(\mathbf{a})$ and $N(\mathbf{a})$ are the values of $\mathbf{d}$ and N satisfying the nonlinear equilibrium condition Eq. (11) for the final load ($\lambda = 1$) and the assigned actuation $\mathbf{a}$. Thus, $\mathbf{d}(\mathbf{a})$ and $N(\mathbf{a})$ are only implicitly defined by the nonlinear equilibrium condition.

Our novel methodology for a closed-form gradient evaluation is based on the so-called implicit differentiation, a strategy in calculus that makes use of the chain rule to differentiate implicitly defined functions. Accordingly, we can differentiate the residual equilibrium equations as

$$\frac{\partial \mathbf{r}(\mathbf{d}(\mathbf{a}), \mathbf{a})}{\partial \mathbf{a}} = \underbrace{\frac{\partial \mathbf{s}(\mathbf{d}, \mathbf{a})}{\partial \mathbf{d}}\bigg|_{\mathbf{d}(\mathbf{a})}}_{\boldsymbol{K}(\mathbf{d}(\mathbf{a}))} \nabla_{\mathbf{a}}\mathbf{d} + \frac{\partial \mathbf{s}(\mathbf{d}, \mathbf{a})}{\partial \mathbf{a}}\bigg|_{\mathbf{d}(\mathbf{a})} = \mathbf{0} \qquad (15)$$

where $\frac{\partial \mathbf{s}(\mathbf{d}, \mathbf{a})}{\partial \mathbf{d}}\bigg|_{\mathbf{d}(\mathbf{a})}$ coincides with the tangent stiffness matrix evaluated at the final iteration of the structural equilibrium Newton solver, while $\frac{\partial \mathbf{s}(\mathbf{d}, \mathbf{a})}{\partial \mathbf{a}}\bigg|_{\mathbf{d}(\mathbf{a})}$ collects the partial derivatives of the internal forces at the final equilibrium Newton iteration with respect to the actuation inputs considering $\mathbf{d}$ independent from $\mathbf{a}$ in the differentiation. This last ingredient can be evaluated by assembling the contribution of each finite element, actuated or not, to the global $\frac{\partial \mathbf{s}(\mathbf{d}, \mathbf{a})}{\partial \mathbf{a}}$ for assigned displacements. This element contribution can be computed as

$$\frac{\partial \mathbf{s}_e(\mathbf{d}_e, a_e)}{\partial a_e} = \frac{\partial N_e(\mathbf{d}_e, a_e)}{\partial a_e} \mathbf{q}_e(\mathbf{d}_e) \quad \text{with} \quad \frac{\partial N_e(\mathbf{d}_e, a_e)}{\partial a_e} = \begin{cases} -\dfrac{EA}{L_e} & \text{if } a_e \neq 0 \\ 0 & \text{if } a_e = 0 \end{cases} \qquad (16)$$

Eq. (15) provides a way to compute directly and in closed form $\nabla_{\mathbf{a}}\mathbf{d}$ by solving the linear system:

$$\boldsymbol{K}(\mathbf{d}(\mathbf{a})) \nabla_{\mathbf{a}}\mathbf{d} = -\frac{\partial \mathbf{s}(\mathbf{d}, \mathbf{a})}{\partial \mathbf{a}}\bigg|_{\mathbf{d}(\mathbf{a})} \qquad (17)$$

This strategy is computationally very interesting since it requires:

- the computation of vector $\frac{\partial \mathbf{s}(\mathbf{d}, \mathbf{a})}{\partial \mathbf{a}}$ that has the same cost of evaluating the internal force vector, even lower because the equilibrium operator $\mathbf{q}_e$ is already available at the last iteration of the structural Newton solver;
- the solution of a linear system in Eq. (17) with a tangent stiffness matrix $\boldsymbol{K}(\mathbf{d}(\mathbf{a}))$ already available and factorized at the last iteration of the structural Newton solver.

Compared to the numerical gradient evaluation requiring multiple nonlinear structural analyses, this strategy gives an exact algorithmic gradient at practically no cost.

It is interesting to note, as a mechanical interpretation, that $\frac{\partial \mathbf{s}(\mathbf{d}, \mathbf{a})}{\partial \mathbf{a}}$ involves the derivative of the axial force of the generic element for assigned displacement with respect to the actuation of the element itself. The actuation inputs in the other elements do not contribute to this term. The fact that varying the actuation in one element can affect the displacements in all structural nodes comes from the coupling in the tangent stiffness matrix.

Once the gradient of the displacements is computed, the gradient of the axial force N_e in the generic bar e can be then evaluated by the chain rule as

$$\nabla_{\mathbf{a}}N_e = \frac{\partial N_e(\mathbf{d}_e, a_e)}{\partial \mathbf{d}_e}\bigg|_{\mathbf{d}_e(\mathbf{a})} \nabla_{\mathbf{a}}\mathbf{d}_e + \frac{\partial N_e(\mathbf{d}_e, a_e)}{\partial a_e}\bigg|_{\mathbf{d}_e(\mathbf{a})} \qquad (18)$$

where $\frac{\partial N_e(\mathbf{d}_e, a_e)}{\partial \mathbf{d}_e} = \frac{EA}{L_e}\mathbf{q}_e(\mathbf{d}_e)^T$ and $\nabla_{\mathbf{a}}\mathbf{d}_e$ is the element version of $\nabla_{\mathbf{a}}\mathbf{d}$ obtained by extracting the values in the positions corresponding to the nodal DOFs of the generic element e. By substituting, we have explicitly

$$\nabla_{\mathbf{a}}N_e = \frac{EA}{L_e}\mathbf{q}_e(\mathbf{d}_e(\mathbf{a}))^T \nabla_{\mathbf{a}}\mathbf{d}_e + \frac{\partial N_e(\mathbf{d}_e, a_e)}{\partial a_e}\bigg|_{\mathbf{d}_e(\mathbf{a})}. \qquad (19)$$

Again, considering the right hand of Eq. (19), we can observe that the second term takes into account the variation of the axial force of each element with respect to its actuation, while the fact that varying the actuation in one element can affect the stress in all the others is recovered by the first term due to the displacement gradient.

3.4. Remarks

It is worth highlighting that all discrete operators needed in the proposed gradient evaluation strategy are already implemented in structural finite element codes. This means that the exact gradient can be computed with minimal implementation changes directly at the final step of the incremental nonlinear analysis. Indeed, the same routines already available for computing the internal force vector and the element stress can be directly reused for evaluating the partial derivatives of the internal force vector and element stress in Eq. (16) by simply giving different input data. Furthermore, It is interesting to note that multiple load cases can be directly managed in the proposed framework by simply duplicating displacement and stress constraints for each.

4. Results and discussion

In this section, we have implemented the methodology developed in the previous section on various examples, considering displacement and axial force control both independently and in conjunction. The validity of the presented technique has been verified by comparing the obtained results with those described in the literature.
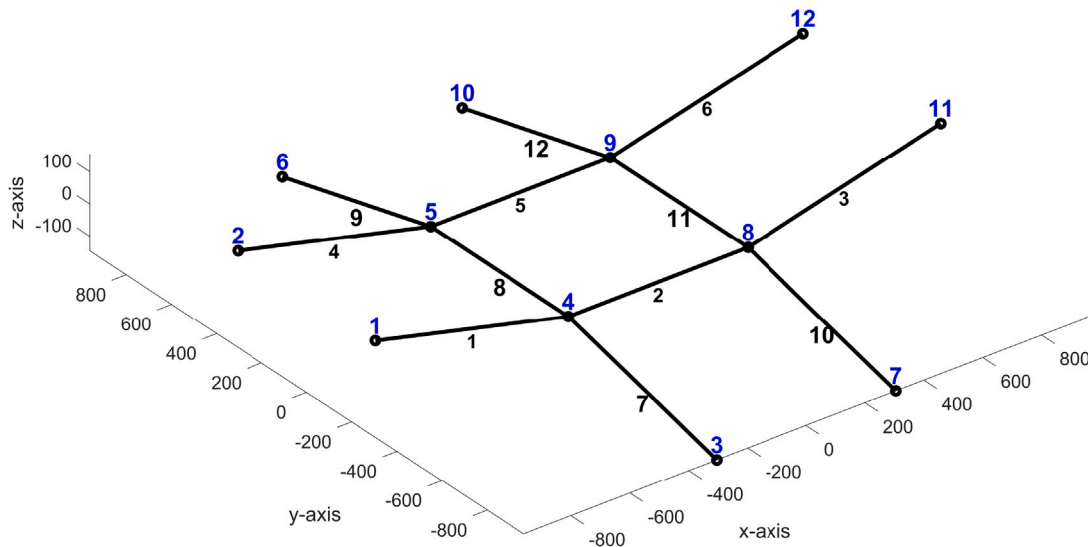
Fig. 2. Geometry of a saddle-shaped cable net structure [55].

Table 1

Displacement control of a saddle-shaped cable net structure: pre (p) and post(a) adjustment.

Joint	Dir.	d_p (mm)	d_a (mm)	Cable	a (mm)	N_p (N)	N_a (N)
	x	−0.62	−0.03	1	4.73	143.9	85.6
4	y	0.59	1.27	2	0.00	139.6	83.3
	z	−8.84	−20.00	3	4.73	143.9	85.6
	x	−0.62	−0.03	4	4.73	143.9	85.6
5	y	−0.59	−1.27	5	0.00	139.6	83.3
	z	−8.84	−20.00	6	4.73	143.9	85.6
	x	0.62	0.03	7	0.00	24.4	−41.5
8	y	0.59	1.27	8	0.00	24.0	−40.6
	z	−8.84	−20.00	9	0.00	24.4	−41.5
	x	0.62	0.03	10	0.00	24.4	−41.5
9	y	−0.59	−1.27	11	0.00	24.0	−40.6
	z	−8.84	−20.00	12	0.00	24.4	−41.5
				$\sum a_i = 18.92$			

4.1. Saddle-shaped cable net structure

Fig. 2 illustrates a 3-D cable net featuring twelve nodes and cables made of piano wire (42 mm diameter, 210 MPa modulus of elasticity, and 2000 MPa tensile strength). The cable net is restrained at the circumference joints, while the mid joints remain unrestrained. This structure, subjected to testing by [53] and analyzed numerically by [54], is both statically and kinematically indeterminate. Initial prestressing, following Pellegrino's recommendation [53], is applied by actuating cables $1, 3, 4, 6, 7, 9, 10$, and 12 with a displacement of -1.85 mm, and cables $2, 5, 8$, and 11 with a displacement of -1.68 mm. Additionally, the free nodes are loaded with 30 N in the downward direction.

Table 1 presents the nodal displacements resulting from external loading, with the objective of positioning the free nodes at a displacement of -20 mm. The table indicates the successful achievement of this goal through the actuation of only four cables. Since the primary focus in this phase is on nodal positions, axial forces were intentionally disregarded, resulting in slack in certain cables.

In the second step, the saddle cable shown in Fig. 2 and the same initial prestress and external loading were examined to control the axial forces in the cables within $10 \text{ N} \leq N_e \leq 125 \text{ N}$ to keep them from slacking and high stress. The target axial forces N_a and the actuation values are reported in Table 2. Since the nodal position of the joints was not considered, the vertical displacement of the free joints after cable actuation became -17.12 mm each.

Table 2

Stress control of a saddle-shaped cable net structure: pre (p) and post(a) adjustment.

Cable	a (mm)	N_p (N)	N_a (N)
1	2.687	143.9	125.0
2	0.000	139.6	121.4
3	2.687	143.9	125.0
4	2.687	143.9	125.0
5	0.000	139.6	121.4
6	2.687	143.9	125.0
7	−0.881	24.4	10.0
8	−0.575	24.0	10.0
9	−0.881	24.4	10.0
10	−0.881	24.4	10.0
11	−0.575	24.0	10.0
12	−0.881	24.4	10.0
$\sum |a_i| = 15.422$			

For the current example, when considering only the nodal positions, some cables experience slackness, rendering the structure unstable as cables can only carry tension [56]. Conversely, when focusing solely on axial forces, the nodes assume arbitrary positions, as demonstrated earlier. Now, the structures (Fig. 2) is examined to control nodal positions and axial forces in cables simultaneously. Sometimes, it is essential to maintain both shape and stress simultaneously.

In this case, both shape and stress are taken into account: the objective is to set the free nodes to a -20 mm vertical displacement while keeping the axial force on the elements N_e within the range of

Table 3
Displacement and axial force control of a saddle-shaped cable net structure: pre (p) and post (a) adjustment.

Joint	Direction	d_p (mm)	d_a (mm)	Cable	a (mm)	N_p (N)	N_a (N)
4	X	−0.62	−0.03	1	3.50	143.9	122.8
	Y	0.59	1.27	2	0.00	139.6	119.3
	Z	−8.84	−20.00	3	3.50	143.9	122.8
5	X	−0.62	−0.03	4	3.50	143.9	122.8
	Y	−0.59	−1.27	5	0.00	139.6	119.3
	Z	−8.84	−20.00	6	3.50	143.9	122.8
8	X	0.62	0.03	7	−0.93	24.4	10.0
	Y	0.59	1.27	8	−1.59	24.0	10.1
	Z	−8.84	−20.00	9	−0.93	24.4	10.0
9	X	0.62	0.03	10	−0.93	24.4	10.0
	Y	−0.59	−1.27	11	−1.59	24.0	10.1
	Z	−8.84	−20.00	12	−0.93	24.4	10.0
				$\sum |a| =$	20.91		

Table 4
Reduction of the computational cost by analytical gradient for displacement control.

Gradient	Iterations		Structural analyses	
	Numerical	Analytical	Numerical	Analytical
Displacement control	4	4	29	9
Stress control	15	15	440	265
Displacement and stress control	16	13	522	251

Table 5
Axial force (N) control of a space cable structure.

Members	Initial stage	After loading	After actuation			
			Case 1		Case 2	
			[21]	Present	[21]	Present
Strut	−28 140	−38 250	−47 260	−47 225	−48 150	−48 152
Upper cable	29 010	19 140	29 010	29 010	29 010	29 010
Lower cable	29 010	38 780	47 240	47 134	49 660	49 642

$10 \text{ N} \leq N_e \leq 125 \text{ N}$. Table 3 displays the displacements and axial forces in cables before and after applying the set of actuations obtained from the current technique. It is evident that the targets were precisely achieved by actuating ten cables with 20.91 mm.

4.1.1. Reduction of the computational cost

To achieve a reduction in computational cost by leveraging analytical gradients for nonlinear constraint functions, Table 4 provides a comparative analysis of the number of iterations and function/constraint evaluations (structural analyses) for the saddle-shaped cable net structure, considering displacement, stress, and coupled control. Significantly, utilizing the present analytical gradients of the nonlinear finite element solution results in substantially fewer iterations and structural analyses compared to numerical gradients.

Specifically, for displacement control alone, the numerical data reveals that the number of structural analyses using analytical gradients are lower by 68.9%, compared to those using numerical gradients. This indicates that the proposal not only avoids the need for multiple nonlinear structural analyses to compute the gradient but also enhances the accuracy of the gradient itself, leading to improved convergence of the optimization algorithm.

4.2. Space cable structure

Fig. 3 presents the numerical example which was previously investigated by Yuan et al. [21] and which is used in this study to validate the effectiveness of the present method in handling geometrically nonlinear structures. The structure comprises of four restrained and two free joints, a vertical strut with a hollow circular section ($\varnothing 50 \times 4$ mm, elastic modulus of 206 GPa) connecting the top and bottom free joints. Additionally, eight cables with a diameter of 8 mm and elastic modules of 185 GPa are incorporated. The initial axial force in the strut is of −28, 140 N, while for the upper and lower cables, it is set as equal to 19,01 N. Application of a 20,00 N downward force at the top free joint results in a −9.00 mm displacement in the Z direction and changing the axial force in the strut, upper and lower cables to −38 249, 19 140, and 38 775 N respectively.

This case aims to nullify the top free joint's X, Y, and Z displacements. Yuan, Liang [21] addressed this by extending the upper cables by 4.56 mm to control the nodal displacement of the top free joint. A comparable result was achieved to validate the accuracy of the current

approach, the target was achieved by actuating the upper cables by 5.57 mm, which demonstrating a mere 0.2% dissimilarity with the previous study.

The same structural configuration (Fig. 3) undergoes testing to validate the developed technique emphasizing axial force control regardless of displacement. Table 5 overviews the induced axial forces in members after the initial stage and applied loads. The objective is to maintain the internal force in the upper cables at their initial stage (29 010 N), employing two distinct scenarios of cable actuation. In Case 1, only the top cables are actuated, while in Case 2, solely the bottom cables are actuated to sustain the axial force in the top cables. A comparative analysis between the study's results by Yuan et al. [21] and the current investigation reveals that the targets were successfully achieved in both cases, with a slight dissimilarity in the amount of actuation. It should be noted that, for Case 1, the previous study requires shortening the upper cables by 4.03 mm, while the current research asks to shorten the cables by 3.96 mm. This indicates that the current approach achieves the target with 1.7% less actuation effort compared to the previous work, highlighting improved efficiency. Moreover, this reduction in actuation was achieved without compromising the cost-effectiveness of identifying the optimal solution.

4.2.1. Reduction of the computational cost

The efficiency of the advanced optimization, based on analytical gradients for nonlinear constraint functions (displacement and stress), is assessed in Table 6. This table presents the number of iterations and function/constraint evaluations (structural analyses) for the space cable structure, considering both displacement and stress control. The utilization of the present analytical gradients for the nonlinear finite element solution results in significantly fewer iterations and structural analyses compared to numerical gradients. Specifically, for displacement control, the algorithm requires a reduction of 82.9% in the number of function/constraint evaluations using the new analytical gradients compared to those using numerical gradients.

4.3. A 2D cable net

This example validates the present approach for controlling axial force and large displacement in a 2D cable net structure (depicted in Fig. 4). The cable structure underwent experimental testing by
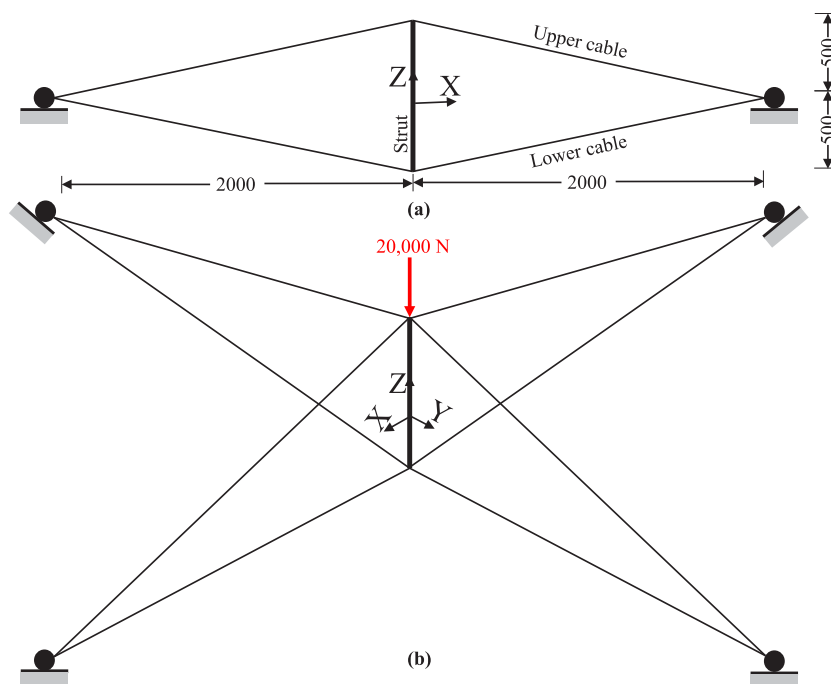
Fig. 3. Space cable structure (a) Front view (b) 3D view [21].

Table 6
Reduction of the computational cost by analytical gradient for controlling the space cable structure.

Gradient	Iterations		Structural analyses	
	Numerical	Analytical	Numerical	Analytical
Displacement control	4	3	41	7
Stress control	4	3	47	21

You [16] for displacement control in prestressed systems. Subsequent investigations by Xu and Luo [57] as well as Saeed [58] delved into controlling shape and stress in nonlinear cable configurations.

The structure consists of three free and four restrained joints, with nine cables featuring $EA = 43160$ N. The initial axial force in cables N_0 is specified in Table 7.

The primary objective is to impart $[-20, 20]$ mm displacement to the X and Y coordinates, respectively, of Joint 6 while maintaining the stress in the cables as close as possible to their initial levels. In particular, we impose that the axial forces of the cables are exactly the target ones N_0. The problem so formulated could be not feasible. In this case, the optimization algorithm stops when the feasibility error stop decreasing. This solution is then accepted as the closest one to the target problem. Xu and Luo [57] successfully achieved the displacement requirement; however, the axial force in some members deviated slightly from the initial values, as outlined in Table 7. Noteworthy differences between the target and induced axial forces after actuation in the study by Xu and Luo [57] are observed in cables iii, iv, and vii, with discrepancies of 21.8%, 19.4%, and 19.1%, respectively.

In the current study, despite precisely achieving the target displacement, the maximum discrepancy between the target axial force and the post-actuation induced force occurred in Cable v, amounting to 11.5%. The current approach uses fewer actuations by 28.7% compared to the previous method.

The same model was investigated with varying control requirements. The cable net was prestressed by applying elongation of $[-5.02, 4.49, -5.02]$ mm to Cables vii, viii, and ix, respectively. This resulted in nodal displacements and axial forces, as detailed in Table 8. The objective was to eliminate the X and Y displacements of Joint 6,

maintain stress levels above the initial threshold, and utilize only four actuators. All previous studies as well as the present one successfully achieved the specified targets. Shen et al. [59], Saeed et al. [17] and Saeed [58] required 18.6, 18.3, and 18.1 mm of actuation, respectively, to attain the targeted displacements and maintain stress above the initial level. The present approach accomplished the goal using 17.9 mm of actuation as detailed in Table 8.

Table 9 displays the iteration counts and the number of structural analyses for two cases of displacement and stress control employing numerical and analytical gradients of the nonlinear constraints. An outstanding reduction in iterations and function evaluations is evident when utilizing the new closed-form gradients compared to numerical ones. This shows the accuracy of the gradient affects significantly also the iterations of the optimization algorithm. The results of this study demonstrate that the proposed method offers significant advantages over previous approaches. Specifically, it minimizes the objective function while strictly adhering to the imposed constraints. Moreover, the method is computationally efficient, making it a more cost-effective solution than existing alternatives which use numerical gradients.

4.4. Deployable space truss

Fig. 5 illustrates a fully opened deployable truss comprising 25 nodes and 60 bars. Nodes 1, 5, 9, 16, 20, 24, and 25 are restrained in all directions. Cables 1–33 have $EA = 98$ kN, while struts 34–60 have $EA = 350$ kN, with horizontal and vertical elements measuring 500 mm long. Additionally, Fig. 6 displays the self-stress state of a unit.

The objective is to achieve a prestressing level of 2 N for Cables 3, 5, 7, 8, 11, and 1 N for the remaining cables, along with −1 N for the struts, as outlined in Table 10. This is to be accomplished by actuating only Cables 1, 3, 4, 7, 8, and 9.

In a study by Kwan and Pellegrino [53], the goal was achieved with a total actuation of 0.4861 mm, while Abdulkarim and Saeed [20] accomplished it with a total actuation of 0.4755 mm. However, with the current approach, the target can be met with 0.4754 mm, representing a 3.23% and 1.07% reduction compared to the studies by Kwan and Pellegrino [53] and by Abdulkarim and Saeed [20], respectively.
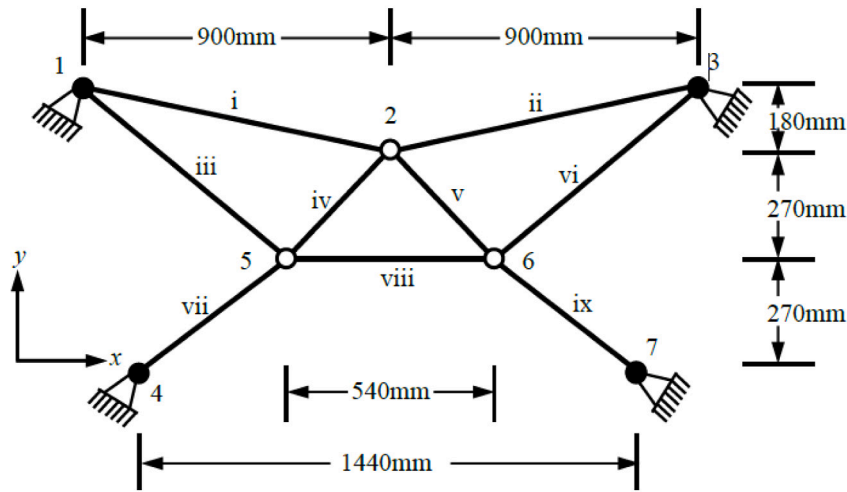
Fig. 4. A 2D cable net.

Table 7

Imparting [−20 20] mm displacement to the X and Y coordinates, respectively, of Joint 6 of the 2D cable net while maintaining the stress in the cables as close as possible to their initial levels N_0.

Cable	N_0 (N)	[57]			Current study		
		N_a (N)	Error (%)	a (mm)	N_a (N)	Error (%)	a (mm)
i	61.4	63.9	4.1	−14.360	61.6	0.4	0.02
ii	61.4	59.7	2.7	11.130	61.6	0.3	−0.02
iii	23.6	18.4	21.8	9.520	23.5	0.0	−9.80
iv	17.0	13.7	19.4	11.800	17.0	0.1	0.16
v	17.0	18.3	7.7	−13.300	19.0	11.5	−27.28
vi	23.6	28.0	19.1	4.940	24.7	5.0	5.14
vii	50.0	51.0	2.1	−10.620	50.0	0.0	−2.34
viii	50.0	50.4	0.8	−16.910	50.0	0.0	−12.61
ix	50.0	46.9	6.1	27.560	45.2	9.7	28.26
Total actuation (mm)				120.1			85.6
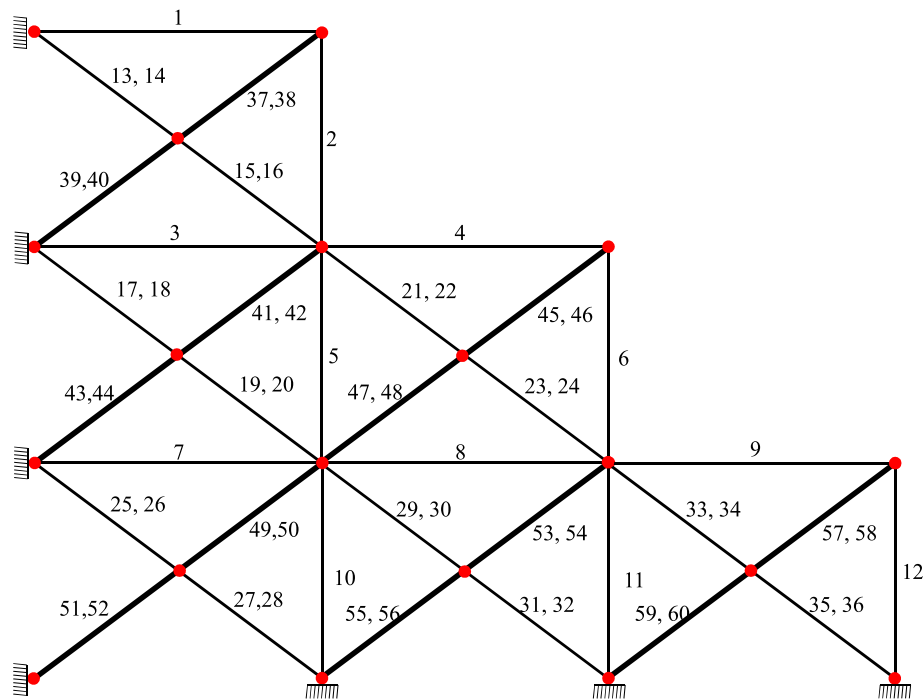
Fig. 5. Deployable space truss.

Table 8
Eliminating nodal displacements of Joint 6 and keeping the stress above the initial level of the 2D cable net with four actuators.

Cable	N_p (N)	[58]		Current study	
		N_a (N)	a (mm)	N_a (N)	a (mm)
i	61	120	0	125	0
ii	61	119	0	117	0
iii	23	23.6	0	23.6	0
iv	17	33.8	0	31.7	0
v	17	34.9	−9.2	43.2	−9.24
vi	23	26.6	−0.4	23.6	−0.42
vii	50	73.1	−4.3	73.6	−4.21
viii	50	57.9	0	58.0	0
ix	50	74.1	4.2	81.5	4.03
Total actuation (mm)			18.1		17.9

Table 9
Reduction of the computational cost by analytical gradient for simultaneous displacement and stress control of the 2D cable net.

Gradient	Iterations		Structural analyses	
	Numerical	Analytical	Numerical	Analytical
Control case 1	156	10	3017	60
Control case 2	23	5	221	11
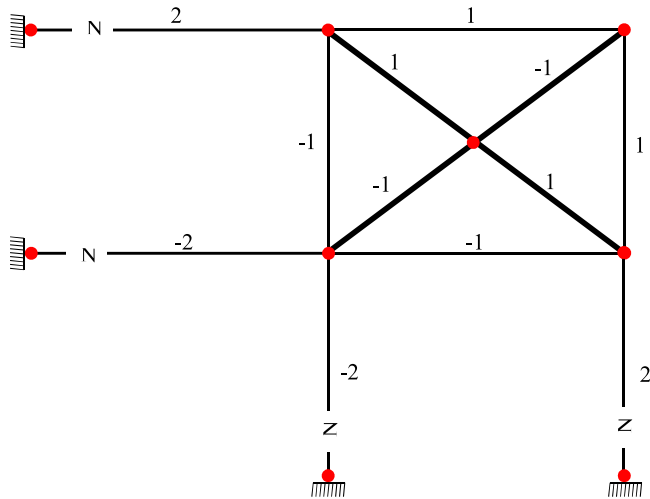
Fig. 6. Self stress state of a unit of the deployable space truss.

Table 10
Prestressing the deployable space truss.

Members	N_{target} (N)	[53]	[20]	Current
1	1	−0.1550	−0.1513	−0.1547
3	2	−0.0931	−0.0867	−0.0930
4	1	0.1238	0.1270	0.1236
7	2	−0.0415	−0.0336	−0.0414
8	2	0.0312	0.0391	0.0312
9	1	−0.0415	−0.0378	−0.0265
5,10,11	2	–	–	–
2,6,12–36	1	–	–	–
37–60	−1	–	–	–
Total actuation (mm)		0.4861	0.4755	0.4704

In this test, the closed-form differentiation of the structural response with respect to the actuation inputs notably reduces the number of structural analyses required to evaluate the nonlinear constraints, such as axial forces, as presented in Table 11. The table illustrates that employing the analytical gradient for both the objective and constraint functions reduces up to 85% in computational effort compared to using a numerical gradient. These findings indicate that the proposed

Table 11
Reduction of the computational cost by analytical gradient for stress control of the deployable space truss.

Gradient	Iterations		Structural analyses	
	Numerical	Analytical	Numerical	Analytical
Stress control	3	3	40	6

approach achieves a lower objective function value than previous methods and meets the target goals more computationally efficient and cost-effective manner.

4.5. Large plate-like truss

This final test involves a large plate-like statically indeterminate truss, depicted in Fig. 7. The plate is divided into 10 a modules along each edge, each having a rectangular cuboid shape delimited by horizontal and vertical bars along the 12 edges, with additional diagonal bars in the faces. The members are made of steel with a modulus of elasticity of 210 MPa and an area of 500 mm². The structure comprises 1401 bars and 242 nodes, resulting in a total of 726 nodal displacement degrees of freedom (DOFs). All displacement components are restrained along the top external perimeter of the plate. Additionally, all nodes on the bottom surface are loaded with a vertical downward force of 3 kN. In its initial, unactuated configuration, the structure exhibits a maximum axial force of 112.75 kN. The optimization goal is to minimize the total actuation in the 28 bars highlighted in red in Fig. 7, subject to the following constraints: (i) the absolute value of actuation in each bar is limited to 1.5 mm; (ii) the axial force in each bar is limited to 80 kN in absolute value. These nonlinear constraints involve the axial forces of all 1401 structural elements. The optimal actuation, found by the algorithm, is symmetric (up to machine precision) with respect to the center of the plate and is depicted in Fig. 8. As expected, this actuation reduces the maximum axial force to 80 kN. Conducting the analysis with the same actuation but neglecting the geometric nonlinearity results in a maximum axial force of 102.98 kN, confirming the actual nonlinear behavior of this structure. For this test, the closed-form differentiation strategy allows us to obtain the optimum in just 21 s, compared to the 298 s required by default numerical differentiation. The ratio of the computational time is similar to the ratio of structural analyses (see Table 12), demonstrating how the cost of analytical differentiation is negligible for large structures compared to the structural analysis itself, thanks to the exploitation of the already factorized tangent stiffness matrix.

5. Final discussion, conclusions and outlook

This paper introduced a gradient-based optimization approach for designing actuation systems capable of achieving desired shape and stress control in geometrically nonlinear structures. The actuation is modeled as prescribed deformations in the actuated structural elements, with 3D trusses serving as examples in the application. In typical gradient-based nonlinear optimization, numerical gradient approximation is needed, which can significantly contribute to the overall computational cost. In contrast, this work presents an innovative approach by developing analytical differentiation of the nonlinear finite element solution, considering both displacement and stress with respect to the actuation input parameters. This approach allows for the computation of an exact and cost-effective gradient within the structural analysis. The proposal was presented in a general finite element setting, showing how straightforward its integration into commercial structural software is. Indeed, all ingredients needed by the present exact gradient evaluation strategy are already available in all finite element codes, so only minimal changes are required. The cost-effectiveness is achieved
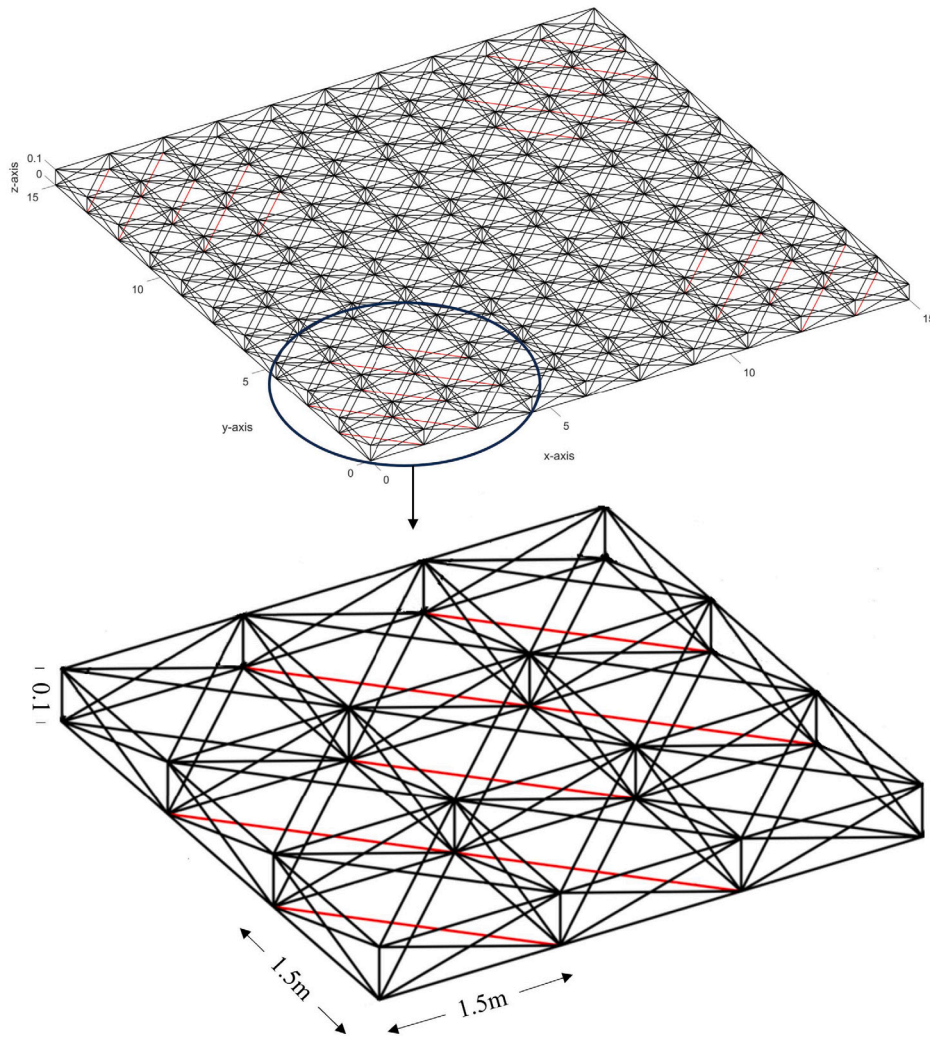
Fig. 7. Large plate-like statically indeterminate truss (lengths in m). (For interpretation of the references to color in this figure legend, the reader is referred to the web version of this article.)

Table 12
Reduction of the computational cost by analytical gradient for stress control of the large plate-like structure.

Gradient	Iterations		Structural analyses		Computational time	
	Numerical	Analytical	Numerical	Analytical	Numerical	Analytical
Stress control	4	4	149	9	298 s	21 s
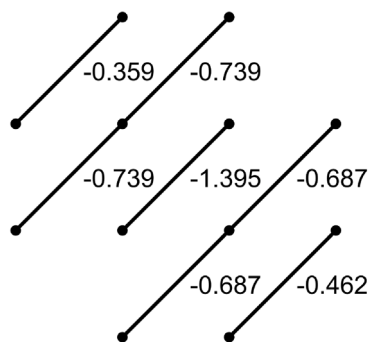
Fig. 8. Optimized actuation in the bars in mm. The solution is symmetric with the plate center located at the bottom left point of this picture.

through a gradient evaluation strategy that leverages the already factorized tangent stiffness matrix during Newton equilibrium iterations. This strategy alone significantly reduces the computational time. Furthermore, the accuracy of the gradient enhances the robustness of the optimization process, reducing, in some cases, the number of iterations required. It is interesting to note the final large structure case, for which the proposed methodology reduced the computational time by about 14 times. The current limitations of this work regard the structural type and the assumption of elastic material. A future development concerns validating the proposal for different structural types, such as beams and shells, for which the present gradient computation is already suitable thanks to the general finite element formalism. Moreover, it would be interesting to extend the exact algorithmic gradient evaluation to nonlinear material, such as plasticity. This seems possible by considering the additional state variables and the loading history through a more involved implicit chain differentiation.

CRediT authorship contribution statement

Declaration of competing interest

The authors declare that they have no known competing financial interests or personal relationships that could have appeared to influence the work reported in this paper.

Acknowledgments

Data availability

Data will be made available on request.

References

[1] Tagai R, Kitamoto K, Hamori H, Mizutani T, Kawashima T, Iwasaki A. High-precision real-time displacement control for large optical system structure. In: Proc. SPIE. Vol. 12486, 2023, 124860E, http://dx.doi.org/10.1117/12.2652282.

[2] Yuan S, Yang B, Fang H. The projecting surface method for improvement of surface accuracy of large deployable mesh reflectors. Acta Astronaut 2018;151:678–90. http://dx.doi.org/10.1016/j.actaastro.2018.07.005.

[3] Lang X, Damaren CJ. Active shape control for flexible space structures using an optimal gyricity distribution. Adv Space Res 2023;71(1):803–15. http://dx.doi.org/10.1016/j.asr.2022.10.049.

[4] Nouri-Baranger T. Computational methods for tension-loaded structures. Arch Comput Methods Eng 2004;11(2):143. http://dx.doi.org/10.1007/BF02905937.

[5] Kawaguchi K-I, Hangai Y, Pellegrino S, Furuya H. Shape and stress control analysis of prestressed truss structures. J Reinf Plast Compos 1996;15(12):1226–36. http://dx.doi.org/10.1177/073168449601501204.

[6] Ziegler F. Computational aspects of structural shape control. Comput Struct 2005;83(15):1191–204. http://dx.doi.org/10.1016/j.compstruc.2004.08.026.

[7] Manguri A, Saeed N, Jankowski R. Controlling nodal displacement of pantographic structures using matrix condensation and interior-point optimization: A numerical and experimental study. Eng Struct 2024;304:117603. http://dx.doi.org/10.1016/j.engstruct.2024.117603, URL https://www.sciencedirect.com/science/article/pii/S0141029624001652.

[8] Song G, Ma N, Li H-N. Applications of shape memory alloys in civil structures. Eng Struct 2006;28(9):1266–74. http://dx.doi.org/10.1016/j.engstruct.2005.12.010.

[9] Irschik H. A review on static and dynamic shape control of structures by piezoelectric actuation. Eng Struct 2002;24(1):5–11. http://dx.doi.org/10.1016/S0141-0296(01)00081-5.

[10] Sunar M, Rao SS. Recent advances in sensing and control of flexible structures via piezoelectric materials technology. Appl Mech Rev 1999;52(1):1–16. http://dx.doi.org/10.1115/1.3098923.

[11] Elefante G, De Bellis ML, Bacigalupo A. Electrically-tunable active metamaterials for damped elastic wave propagation control. Int J Solids Struct 2023;276:112306. http://dx.doi.org/10.1016/j.ijsolstr.2023.112306.

[12] Weeks CJ. Static shape determination and control for large space structures: I. The flexible beam. J Dyn Syst Meas Control 1984;106(4):261–6. http://dx.doi.org/10.1115/1.3140683.

[13] Weeks CJ. Static shape determination and control of large space structures: II. A large space antenna. J Dyn Syst Meas Control 1984;106(4):267–72. http://dx.doi.org/10.1115/1.3140684.

[14] Burdisso RA, Haftka RT. Statistical analysis of static shape control in space structures. AIAA J 1990;28(8):1504–8. http://dx.doi.org/10.2514/3.25245.

[15] Manguri A, Saeed N, Jankowski R. A review: structural shape and stress control techniques and their applications. Arch Comput Methods Eng 2024;1–14. http://dx.doi.org/10.1007/s11831-024-10149-9.

[16] You Z. Displacement control of prestressed structures. Comput Methods Appl Mech Engrg 1997;144(1):51–9. http://dx.doi.org/10.1016/S0045-7825(96)01164-4.

[17] Saeed NM, Kwan ASK. Simultaneous displacement and internal force prescription in shape control of pin-jointed assemblies. AIAA J 2016;54(8):2499–506. http://dx.doi.org/10.2514/1.J054811.

[18] Saeed NM, Manguri AA, Szczepanski M, Jankowski R, Haydar BA. Static shape and stress control of trusses with optimum time, actuators and actuation. Int J Civ Eng 2023;21(3):379–90. http://dx.doi.org/10.1007/s40999-022-00784-3.

[19] Reksowardojo AP, Senatore G. A proof of equivalence of two force methods for active structural control. Mech Res Commun 2020;103:103465. http://dx.doi.org/10.1016/j.mechrescom.2019.103465.

[20] Abdulkarim SJ, Saeed NM. Nonlinear technique of prestressing spatial structures. Mech Res Commun 2023;127:104040. http://dx.doi.org/10.1016/j.mechrescom.2022.104040.

[21] Yuan X, Liang X, Li A. Shape and force control of prestressed cable-strut structures based on nonlinear force method. Adv Struct Eng 2016;19(12):1917–26. http://dx.doi.org/10.1177/1369433216652411.

[22] Rao RV, Taler J. Advanced engineering optimization through intelligent techniques. Springer; 2020.

[23] Christensen PW, Klarbring A. An introduction to structural optimization, vol. 153, Springer Science and Business Media; 2008.

[24] Tan X, Mahjoubi S, Zhang Q, Dong D, Bao Y. A framework for improving bridge resilience and sustainability through optimizing high-performance fiber-reinforced cementitious composites. J Infrastruct Preserv Resil 2022;3(1):18. http://dx.doi.org/10.1186/s43065-022-00067-0.

[25] Cucuzza R, Aloisio A, Domaneschi M, Nascimbene R. Multimodal seismic assessment of infrastructures retrofitted with exoskeletons: insights from the Foggia Airport case study. Bull Earthq Eng 2024;22(6):3323–51. http://dx.doi.org/10.1007/s10518-024-01894-0.

[26] Habashneh M, Cucuzza R, Domaneschi M, Movahedi Rad M. Advanced elasto-plastic topology optimization of steel beams under elevated temperatures. Adv Eng Softw 2024;190:103596. http://dx.doi.org/10.1016/j.advengsoft.2024.103596.

[27] Li X, Zhu J, Wang J, Zhang W. Topology optimization for prestressed cable-truss structure considering geometric nonlinearity. Struct Multidiscip Optim 2023;66(9):201. http://dx.doi.org/10.1007/s00158-023-03646-1.

[28] Cucuzza R, Aloisio A, Rad MM, Domaneschi M. Constructability-based design approach for steel structures: From truss beams to real-world inspired industrial buildings. Autom Constr 2024;166:105630. http://dx.doi.org/10.1016/j.autcon.2024.105630.

[29] Chanekar PV, Chopra N, Azarm S. Optimal actuator placement for linear systems with limited number of actuators. In: 2017 American control conference. ACC, 2017, p. 334–9. http://dx.doi.org/10.23919/ACC.2017.7962975.

[30] Ali A, Ghotbi E, Dhingra AK. Optimum placement of actuators in structural and control design using Stackelberg games. J Vib Control 2015;21(7):1373–82. http://dx.doi.org/10.1177/1077546313494113.

[31] Reksowardojo AP, Senatore G, Smith IFC. Experimental testing of a small-scale truss beam that adapts to loads through large shape changes. Front Built Environ 2019;5. http://dx.doi.org/10.3389/fbuil.2019.00093.

[32] Missoum S, Gurdal Z, Gu W. Optimization of nonlinear trusses using a displacement-based approach. Struct Multidiscip Optim 2002;23(3):214–21. http://dx.doi.org/10.1007/s00158-002-0179-1.

[33] Leonetti L, Garcea G, Magisano D, Liguori F, Formica G, Lacarbonara W. Optimal design of CNT-nanocomposite nonlinear shells. Nanomaterials 2020;10(12). http://dx.doi.org/10.3390/nano10122484.

[34] Liang K, Mu J, Li Z. Thermal-mechanical buckling analysis and optimization of the stringer stiffened cylinder using smeared stiffener based reduced-order models. Comput Math Appl 2023;143:108–18. http://dx.doi.org/10.1016/j.camwa.2023.04.041.

[35] Kennedy GJ, Martins JR. A parallel finite-element framework for large-scale gradient-based optimization of high-performance structures. Finite Elem Anal Des 2014;87:56–73. http://dx.doi.org/10.1016/j.finel.2014.04.011.

[36] Ashtari P, Barzegar F. Accelerating fuzzy genetic algorithm for the optimization of steel structures. Struct Multidiscip Optim 2012;45(2):275–85. http://dx.doi.org/10.1007/s00158-011-0700-5.

[37] Sadollah A, Bahreininejad A, Eskandar H, Hamdi M. Mine blast algorithm for optimization of truss structures with discrete variables. Comput Struct 2012;102–103:49–63. http://dx.doi.org/10.1016/j.compstruc.2012.03.013.

[38] Olivo J, Cucuzza R, Bertagnoli G, Domaneschi M. Optimal design of steel exoskeleton for the retrofitting of RC buildings via genetic algorithm. Comput Struct 2024;299:107396. http://dx.doi.org/10.1016/j.compstruc.2024.107396.

[39] Mahjoubi S, Tan X, Bao Y. Inverse analysis of strain distributions sensed by distributed fiber optic sensors subject to strain transfer. Mech Syst Signal Process 2022;166:108474. http://dx.doi.org/10.1016/j.ymssp.2021.108474.

[40] Tan X, Mahjoubi S, Zou X, Meng W, Bao Y. Metaheuristic inverse analysis on interfacial mechanics of distributed fiber optic sensors undergoing interfacial debonding. Mech Syst Signal Process 2023;200:110532. http://dx.doi.org/10.1016/j.ymssp.2023.110532.

[41] Yu T, Marmo F, Cesarano P, Adriaenssens S. Continuous modeling of creased annuli with tunable bistable and looping behaviors. Proc Natl Acad Sci 2023;120(4). http://dx.doi.org/10.1073/pnas.2209048120.

[42] Liguori FS, Magisano D, Leonetti L, Garcea G. Nonlinear thermoelastic analysis of shell structures: solid-shell modelling and high-performing continuation method. Compos Struct 2021;266:113734. http://dx.doi.org/10.1016/j.compstruct.2021.113734.

[43] Liguori FS, Magisano D, Madeo A, Leonetti L, Garcea G. A Koiter reduction technique for the nonlinear thermoelastic analysis of shell structures prone to buckling. Internat J Numer Methods Engrg 2022;123(2):547–76. http://dx.doi.org/10.1002/nme.6868.

[44] Norouzikudiani R, Lucantonio A, De Simone A. Equilibrium and transient response of photo-actuated liquid crystal elastomer beams. Mech Res Commun 2023;131:104126. http://dx.doi.org/10.1016/j.mechrescom.2023.104126.

[45] Nitti A, Kiendl J, Gizzi A, Reali A, de Tullio MD. A curvilinear isogeometric framework for the electromechanical activation of thin muscular tissues. Comput Methods Appl Mech Engrg 2021;382:113877. http://dx.doi.org/10.1016/j.cma.2021.113877.

[46] Cox B, Groh R, Avitabile D, Pirrera A. Modal nudging in nonlinear elasticity: Tailoring the elastic post-buckling behaviour of engineering structures. J Mech Phys Solids 2018;116:135–49. http://dx.doi.org/10.1016/j.jmps.2018.03.025.

[47] Magisano D, Garcea G. Increasing the buckling capacity with modal geometric "imperfections" designed by a reduced order model. Thin-Walled Struct 2022;178:109529. http://dx.doi.org/10.1016/j.tws.2022.109529.

[48] Magisano D, Garcea G. Sensitivity analysis to geometrical imperfections in shell buckling via a mixed generalized path-following method. Thin-Walled Struct 2022;170:108643. http://dx.doi.org/10.1016/j.tws.2021.108643.

[49] Nocedal J, Wright SJ. Numerical optimization. Springer, http://dx.doi.org/10.1007/978-0-387-40065-5.

[50] Riks E. An incremental approach to the solution of snapping and buckling problems. Int J Solids Struct 1979;15(7):529–51. http://dx.doi.org/10.1016/0020-7683(79)90081-7.

[51] Magisano D, Leonetti L, Garcea G. How to improve efficiency and robustness of the Newton method in geometrically non-linear structural problem discretized via displacement-based finite elements. Comput Methods Appl Mech Engrg 2017;313:986–1005. http://dx.doi.org/10.1016/j.cma.2016.10.023.

[52] Magisano D, Corrado A. New robust and efficient global iterations for large deformation finite element analysis of beams and shells with material nonlinearity. Comput Methods Appl Mech Engrg 2023;406:115900. http://dx.doi.org/10.1016/j.cma.2023.115900.

[53] Kwan A, Pellegrino S. Prestressing a space structure. AIAA J 1993;31(10):1961–3. http://dx.doi.org/10.2514/3.11876.

[54] Manguri A, Saeed N, Kazemi F, Szczepanski M, Jankowski R. Optimum number of actuators to minimize the cross-sectional area of prestressable cable and truss structures. Structures 2023;47:2501–14. http://dx.doi.org/10.1016/j.istruc.2022.12.031.

[55] Kaveh A, Hamedani KB, Hamedani BB. Optimal design of large-scale dome truss structures with multiple frequency constraints using success-history based adaptive differential evolution algorithm. Period Polytech Civ Eng 2023;67(1):36–56. http://dx.doi.org/10.3311/PPci.21147.

[56] Saeed NM, Manguri AAH, Adabar AM. Shape and force control of cable structures with minimal actuators and actuation. Int J Space Struct 2021;36(3):241–8. http://dx.doi.org/10.1177/09560599211045851.

[57] Xu X, Luo YZ. Non-linear displacement control of prestressed cable structures. Proc Inst Mech Eng G 2009;223(7):1001–7. http://dx.doi.org/10.1243/09544100JAERO455.

[58] Saeed NM. Displacement control of nonlinear pin-jointed assemblies based on force method and optimization. AIAA J 2022;60(2):1024–31. http://dx.doi.org/10.2514/1.J060568.

[59] Shen L, Li G, Luo Y. Displacement control of prestressed cable structures. Tongji Daxue Xuebao/J Tongji Univ 2006;34(3):291–5.